MITSUBISHI ELECTRIC RESEARCH LABORATORIES
https://www.merl.com

Continuous-Time Successive Convexification for Passively-Safe Spacecraft Rendezvous on a Near Rectilinear Halo Orbit

Elango, Purnanand; Vinod, Abraham P.; Kitamura, Kenji; Acikmese, Behcet; Di Cairano, Stefano; Weiss, Avishai

TR2026-016 January 14, 2026

Abstract

This paper presents an optimization-based method for spacecraft rendezvous to the Gateway that (i) enforces passive safety and an approach-cone path constraint in continuous time, (ii) satisfies decision-point specifications, and (iii) accounts for NRHO insertion, actuation, and navigation uncertainties via chance constraints and stabilizing feedback. The approach employs sequential convex programming within the continuous-time successive convexification (CT-SCVX) framework, in which continuous-time path constraints are reformulated as isoperimetric integral constraints, thereby decoupling continuous-time feasibility (solution quality) from the chosen time-discretization density. In addition, time dilation is used to treat the actuation time instants as optimization variables. A numerical case study for an NRHO apolune rendezvous to the Gateway, validated through Monte Carlo simulation, demonstrates satisfaction of passive-safety and approach-cone constraints with high probability and with comparable fuel usage to recent NRHO rendezvous studies.

AIAA SciTech Forum 2026

Mitsubishi Electric Research Laboratories, Inc.
201 Broadway, Cambridge, Massachusetts 02139

Continuous-Time Successive Convexification for Passively-Safe Spacecraft Rendezvous on a Near Rectilinear Halo Orbit

Purnanand Elango[1*], Abraham P. Vinod[1†], Kenji Kitamura[2‡], Behçet Açıkmeşe[3§], Stefano Di Cairano[1¶], and Avishai Weiss[1||]

[1]*Mitsubishi Electric Research Laboratories, Cambridge, MA, 02139, USA*
[2]*Mitsubishi Electric Corporation, Amagasaki, Hyogo, 661-8661, Japan*
[3]*University of Washington, Seattle, WA, 98195, USA*

This paper presents an optimization-based method for spacecraft rendezvous to the Gateway that (i) enforces passive safety and an approach-cone path constraint in continuous time, (ii) satisfies decision-point specifications, and (iii) accounts for NRHO insertion, actuation, and navigation uncertainties via chance constraints and stabilizing feedback. The approach employs sequential convex programming within the continuous-time successive convexification (CT-SCvx) framework, in which continuous-time path constraints are reformulated as isoperimetric integral constraints, thereby decoupling continuous-time feasibility (solution quality) from the chosen time-discretization density. In addition, time dilation is used to treat the actuation time instants as optimization variables. A numerical case study for an NRHO apolune rendezvous to the Gateway, validated through Monte Carlo simulation, demonstrates satisfaction of passive-safety and approach-cone constraints with high probability and with comparable fuel usage to recent NRHO rendezvous studies.

Nomenclature

$\mathbb{R}, \mathbb{R}^n$	:	Set of real numbers, n-dimensional real vector space
$\|x\|$	:	Euclidean norm of vector x
$\|x\|_+$	:	Nonnegative part of scalar x: $\max\{x, 0\}$
$\|x\|_+$	:	Euclidean norm of the positive components of vector x
(u, v)	:	Concatenation of vector $u \in \mathbb{R}^n$ and $v \in \mathbb{R}^m$ to form a vector in $\mathbb{R}^{n+m}$
0_n, $0_{n\times m}$	:	Zero vector in $\mathbb{R}^n$, zero matrix in $\mathbb{R}^{n\times m}$
I_n	:	Identity matrix in $\mathbb{R}^{n\times n}$
$\mathrm{blkdiag}(A, B)$	:	Block-diagonal matrix with blocks A and B
$\nabla_j h$	:	Gradient of function h with respect to its jth argument
∇h	:	Gradient of a single-argument function h
$\dot{\square}$	:	Derivative of $\square$ with respect to actual time t: $\frac{\mathrm{d}\square}{\mathrm{d}t}$
$\boldsymbol{x}$	:	Random variable (denoted in boldface)
$\mathcal{N}(\mu, \Sigma)$	:	Gaussian distribution with mean μ and covariance Σ
$\mathbb{E}(\boldsymbol{x})$	:	Expectation of random variable $\boldsymbol{x}$
$\mathbb{P}(g(\boldsymbol{x}) \leq 0)$	:	Probability of the event $g(\boldsymbol{x}) \leq 0$
$Q_n(\beta)$	:	Quantile function of chi-squared distribution with n degrees of freedom at confidence level β

*Research Scientist
†Principal Research Scientist
‡Researcher, Advanced Technology R&D Center
§Professor, William E. Boeing Department of Aeronautics and Astronautics
¶Distinguished Research Scientist
||Senior Principal Research Scientist

I. Introduction

NASA's Artemis IV mission will deploy a space station, known as the Gateway [1], on a near rectilinear halo orbit (NRHO) [2] around the Earth–Moon L2 point. Visiting and servicing spacecraft must rendezvous with the Gateway, a critical maneuver for many space operations [3, 4]. A rendezvous maneuver to the Gateway must (i) satisfy passive safety at all times, (ii) enforce multiple decision points along the trajectory according to specified guidelines [5], (iii) ensure fuel efficiency, and (iv) account for uncertainty arising from various sources (e.g., orbital insertion, actuation error, and navigation measurements). Passive safety is a particularly challenging constraint: it requires that, if the spacecraft thrusters fail completely at any time during the rendezvous, the spacecraft's uncontrolled motion (free drift) remains outside a keep-out zone for a specified time interval [6].

In recent years, passively safe rendezvous on NRHO has received considerable attention. Approaches include center-/unstable-manifold-based design [7, 8]; leveraging natural motion for far-range rendezvous in ephemeris models [9]; six-degree-of-freedom (6-DoF) close-range rendezvous [10]; MPC-based guidance [11]; backward reachable set (BRS) safety constraints [12, 13]; adjoint methods with ephemeris validation [14]; and linear covariance (LinCov) design and analysis under uncertainty [15–18]. Here, our goal is to compute a fuel-optimal rendezvous trajectory, from orbital insertion to the start of the proximity phase, that optimizes actuation time instants and ensures safety at all times in the presence of uncertainty.

Optimization-based methods are well suited for generating trajectories of nonlinear systems subject to complex constraints [19, 20]. They can incorporate constraints related to safety [21, 22], temporal logic [23, 24], and multi-phase dynamics [25, 26]. These methods have been successfully applied across a wide range of spacecraft applications, including rendezvous [27, 28], and can be tailored for resource-constrained, radiation-hardened onboard processors [29, 30]. Recent advances have improved robustness to numerical ill-conditioning caused by orders-of-magnitude differences in trajectory-optimization parameters [31–33]. In addition, optimization-based methods can account for uncertainty through deterministic reformulation of chance constraints [34, 35], covariance steering [36–38], conditional value-at-risk minimization [39], and stochastic reachability [40].

However, existing optimization-based rendezvous methods do not ensure safety at all times. They impose the passive-safety constraint at discrete time nodes, similar to widely used direct shooting and collocation methods for numerical optimal control [19]. These methods either explicitly parametrize the free-drift trajectory [10, 21] or use time samples of the backward reachable sets of the keep-out zone [12], which can lead to inter-sample constraint violations [41] and can significantly increase the size of the trajectory-optimization problem when high accuracy is desired. Furthermore, recent approaches that account for uncertainty in NRHO rendezvous rely on LinCov methods [15–18], that generally do not enforce chance constraints to control the joint probability of satisfying multiple path constraints over the entire maneuver horizon.

In this work, we aim to address all requirements (i)–(iv) on the rendezvous maneuver in a unified framework. While several methods address subsets of these requirements, we are not aware of a single formulation that satisfies them simultaneously. We propose an optimization-based method for spacecraft rendezvous to the Gateway that (i) ensures passive safety at all times and enforces the approach-cone path constraint in continuous time; (ii) satisfies the specifications for key decision points along the rendezvous trajectory; and (iii) accounts for uncertainty due to NRHO insertion, actuation error, and navigation measurements via chance constraints, while employing a stabilizing feedback mechanism to bound the effect of these uncertainties. We leverage a sequential convex programming (SCP) approach, based on the recently proposed continuous-time successive convexification (CT-SCvx) framework [42], in which continuous-time path constraints are converted to integral constraints through an isoperimetric reformulation [43]. Relative to our recent work [13], the proposed approach also optimizes impulse times via time dilation [29, 42]. However, unlike [13], it cannot handle continuous control input parameterizations and does not ensure underburn safety.

The rest of the paper is organized as follows. Section II describes the problem formulation, including the spacecraft dynamical model and the path constraints. Sections III and IV present the optimal control problem and the SCP-based solution approach, respectively. Section IV then provides numerical results for a realistic case study involving the Gateway, and Section V offers concluding remarks.

II. Problem Formulation

This section presents the guidelines and specifications for rendezvous of a spacecraft with the Gateway on NRHO, the spacecraft dynamical and actuation model, and the path constraints imposed on the spacecraft trajectory. We also introduce a reformulation of the path constraints that enables tractable enforcement of their continuous-time satisfaction without resorting to expensive mesh refinement.

A. Specifications for NRHO Rendezvous

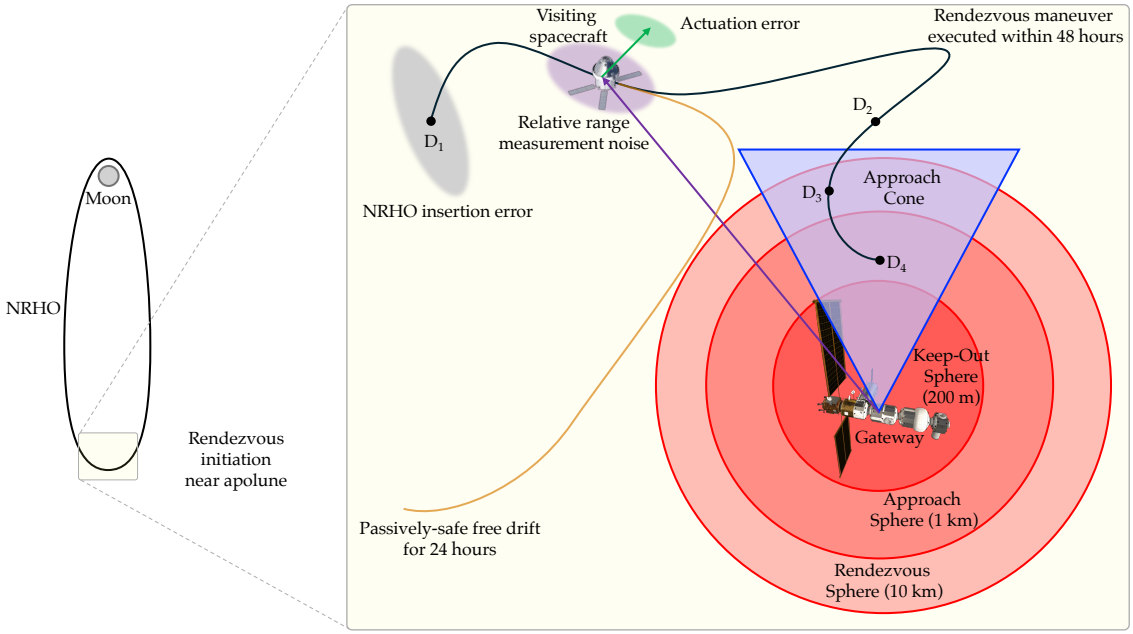

Fig. 1 Schematic of the rendezvous of a spacecraft to the Gateway on NRHO. Figure taken from [13].

We adopt the International Rendezvous System Interoperability Standards (IRSIS) guidelines for rendezvous of a spacecraft with the Gateway on an NRHO [5]. After the spacecraft is inserted onto the NRHO, the rendezvous maneuver starts near the NRHO *apolune*, the farthest point on the NRHO from the Moon, at a distance of 400–2000 km [44] from the Gateway and ends at a point located 500 m from the Gateway. The entire rendezvous maneuver must be completed within 48 hours. The maneuver is divided into three phases, separated by four decision points, denoted D_1–D_4. These phases are defined relative to three nested spherical avoid sets: the rendezvous sphere, the approach sphere, and the keep-out sphere. Specifically, D_1 marks the start of rendezvous after NRHO insertion, D_2 the entry into the rendezvous sphere, D_3 the entry into the approach sphere, and D_4 the start of the proximity phase upon entering the keep-out sphere.

Between D_1 and D_2, the spacecraft must remain passively safe for 24 hours with respect to the rendezvous sphere. That is, in the event of a total failure of the spacecraft thrusters, the free-drift trajectory of the spacecraft must not enter the rendezvous sphere for 24 hours. Between D_2 and D_3, the spacecraft must remain passively safe for 24 hours with respect to the approach sphere, and between D_3 and D_4 it must remain passively safe for 24 hours with respect to the keep-out sphere. The radii of the rendezvous, approach, and keep-out spheres are 10 km, 1 km, and 200 m, respectively. Furthermore, D_4 lies along the Sun–Gateway axis, and the spacecraft must approach the Gateway within an approach cone about this axis to ensure that the Gateway is illuminated and visible to the spacecraft's optical navigation sensors.

We consider three sources of uncertainty in this work: (i) NRHO insertion error, (ii) actuation error in the spacecraft thrusters, and (iii) noise in relative range and range-rate measurements. Figure 1 illustrates the overall maneuver, the decision points, and the sources of uncertainty considered in this work.

The objective is to compute a fuel-efficient rendezvous maneuver that meets all specified requirements and constraints while explicitly accounting for uncertainties. To achieve this, we first describe the spacecraft dy-

namical model, the path constraints, and the discretized optimal control problem for fuel-efficient rendezvous in the deterministic setting. Then we introduce uncertainties to formulate a stochastic optimal control problem and develop an SCP-based solution approach.

B. Spacecraft Dynamical & Actuation Model

The (uncontrolled) natural motion of the spacecraft, also referred to as the *free drift*, is governed by gravitational accelerations from the Moon, Earth, and Sun, along with higher-order effects such as solar radiation pressure (SRP) and the Moon's J_2 perturbation. This motion can be expressed in a Gateway-centered inertial frame as

$$\dot{x}(t) = f(t, x(t)), \tag{1}$$

where the state $x(t) = (r(t), v(t)) \in \mathbb{R}^6$ consists of the spacecraft position $r(t) \in \mathbb{R}^3$ and velocity $v(t) \in \mathbb{R}^3$. A complete description of the dynamical model used in this work is provided in [13].

We assume an impulsive thruster model with at most N velocity impulses applied over a finite time horizon $[0, t^{\mathrm{f}}]$, referred to as the *maneuver horizon*. The impulses occur at time instants

$$0 = t_1 < \ldots < t_N = t^{\mathrm{f}},$$

where $t_2, \ldots, t_N$ are decision variables. The decision points D_1, D_2, D_3, and D_4 occur at time instants t_{N_1}, t_{N_2}, t_{N_3}, and t_{N_4}, respectively, where $1 = N_1 < N_2 < N_3 < N_4 = N$ are fixed integers.

C. Path Constraints

The spacecraft is required to approach the Gateway from within a specified approach cone and to maintain *passive safety* throughout the rendezvous maneuver. First, the approach-cone constraint requires that the spacecraft approaches the Gateway from within a cone with specified axis e^{ac} and half-angle θ^{ac}, i.e.,

$$\cos\theta^{\mathrm{ac}} \|r(t)\| \leq r(t)^\top e^{\mathrm{ac}}. \tag{2}$$

Since the Euclidean norm is non-differentiable at the origin, we rewrite (2) using a differentiable vector-valued path-constraint function g^{ac} as

$$g^{\mathrm{ac}}(r(t)) \triangleq \begin{bmatrix} \|\cos\theta^{\mathrm{ac}} r(t)\|^2 - (r(t)^\top e^{\mathrm{ac}})^2 \\ -r(t)^\top e^{\mathrm{ac}} \end{bmatrix} \leq 0_2. \tag{3}$$

Next, we consider the *passive-safety* constraint, which requires that, in the event of a total failure of the spacecraft thrusters at any time instant during the rendezvous maneuver, the free-drift trajectory of the spacecraft must not enter a specified avoid set around the Gateway for a specified duration t^{s}, referred to as the *safety duration*. The rendezvous, approach, and keep-out sets are modeled as spheres of radii a^{rs}, a^{as}, and a^{kos}, respectively, centered at the origin.

For a given $t \in [0, t^{\mathrm{f}}]$, let the corresponding spacecraft state be $x(t)$. The free-drift trajectory over the safety horizon $[t, t + t^{\mathrm{s}}]$ starting from $x(t)$ is obtained by solving the initial-value problem

$$\frac{\mathrm{d}\check{x}(\gamma, t, x(t), t^{\mathrm{s}})}{\mathrm{d}\gamma} = f(t + \gamma, \check{x}(\gamma, t, x(t), t^{\mathrm{s}})), \quad \gamma \in [0, t^{\mathrm{s}}], \tag{4a}$$

$$\check{x}(0, t, x(t)) = x(t), \tag{4b}$$

where $\check{x}(\gamma, t, x(t), t^{\mathrm{s}})$ is the state at time $t + \gamma$ along the free-drift trajectory starting from $x(t)$. The corresponding position (i.e., the first three components) is denoted $\check{r}(\gamma, t, x(t), t^{\mathrm{s}})$. According to the specification in Section II.A, the passive-safety constraint can be stated as

$$\|\check{r}(\gamma, t, x(t), t^{\mathrm{s}})\| \geq a^{\mathrm{rs}}, \qquad \forall\, \gamma \in [0, t^{\mathrm{s}}], \ \forall\, t \in [t_{N_1}, t_{N_2}], \tag{5a}$$

$$\|\check{r}(\gamma, t, x(t), t^{\mathrm{s}})\| \geq a^{\mathrm{as}}, \qquad \forall\, \gamma \in [0, t^{\mathrm{s}}], \ \forall\, t \in (t_{N_2}, t_{N_3}], \tag{5b}$$

$$\|\check{r}(\gamma, t, x(t), t^{\mathrm{s}})\| \geq a^{\mathrm{kos}}, \qquad \forall\, \gamma \in [0, t^{\mathrm{s}}], \ \forall\, t \in (t_{N_3}, t_{N_4}]. \tag{5c}$$

D. Continuous-Time Constraint Satisfaction

The approach-cone and passive-safety constraints described above must hold at all times over the maneuver horizon, which poses a challenge for numerical optimal control methods that discretize the trajectory and impose the constraints only at discrete time instants. Next, we present computationally tractable reformulations of the approach-cone and passive-safety constraints that ensure their satisfaction in continuous time. Owing to the choice of an impulsive thruster model, we also show that the reformulated constraints can be expressed solely as functions of the spacecraft states immediately before and after each impulse, i.e., $x(t_k^-)$ and $x(t_k^+)$ for $k = 1, \ldots, N$.

We first consider the approach-cone constraint in (3). Imposing this condition only at discrete time instants can lead to inter-sample constraint violations. To enforce continuous-time satisfaction in a tractable manner, we use the isoperimetric reformulation

$$g^{\mathrm{ac}}(r(t)) \leq 0_2, \ \ \forall\, t \in [0, t^{\mathrm{f}}] \iff \int_0^{t^{\mathrm{f}}} \|g^{\mathrm{ac}}(r(t))\|_+^2 \mathrm{d}t = 0. \tag{6}$$

The single integral constraint in (6) ensures satisfaction of the approach-cone constraint at all times over the maneuver horizon. Since we assume an impulsive thruster model, the spacecraft trajectory is in free drift between impulse time instants. Therefore, by leveraging the notation for the free-drift position trajectory introduced in (5), we can rewrite the integral constraint in (6) as

$$\int_0^{t_{k+1}-t_k} \|g^{\mathrm{ac}}(\check{r}(\gamma, t_k, x(t_k^+), t_{k+1} - t_k))\|_+^2 \mathrm{d}\gamma = 0, \ \ k = 1, \ldots, N-1. \tag{7}$$

Next we consider the passive-safety constraint. We require continuous-time safety over both the maneuver and safety horizons. First, to ensure continuous-time satisfaction of the passive-safety constraint across the safety horizon we use again an isoperimetric reformulation

$$\|\check{r}(\gamma, t, x(t), t^{\mathrm{s}})\| \geq a^{\square}, \ \ \forall\, \gamma \in [0, t^{\mathrm{s}}] \iff \Gamma(t, x(t), a^{\square}) \triangleq \int_0^{t^{\mathrm{s}}} \|(a^{\square})^2 - \|\check{r}(\gamma, t, x(t), t^{\mathrm{s}})\|^2\|_+^2 \mathrm{d}\gamma = 0, \tag{8}$$

where $\square \in \{\mathrm{rs}, \mathrm{as}, \mathrm{kos}\}$ depending on the choice of t as specified in (5). Next, observe that, due to the impulsive thruster model, it suffices to impose the passive-safety constraint on the states immediately before and after each impulse. Thus, (5) can be equivalently stated as

$$\Gamma(t_k, x(t_k^+), a^{\mathrm{rs}}) = 0, \quad \Gamma(t_k, x(t_k^-), a^{\mathrm{rs}}) = 0, \quad k = N_1, \ldots, N_2, \tag{9a}$$
$$\Gamma(t_k, x(t_k^+), a^{\mathrm{as}}) = 0, \quad \Gamma(t_k, x(t_k^-), a^{\mathrm{as}}) = 0, \quad k = N_2 + 1, \ldots, N_3, \tag{9b}$$
$$\Gamma(t_k, x(t_k^+), a^{\mathrm{kos}}) = 0, \quad \Gamma(t_k, x(t_k^-), a^{\mathrm{kos}}) = 0, \quad k = N_3 + 1, \ldots, N_4. \tag{9c}$$

For convenience of notation in the subsequent development, we define

$$a_k \triangleq \begin{cases} a^{\mathrm{rs}}, & k = N_1, \ldots, N_2, \\ a^{\mathrm{as}}, & k = N_2 + 1, \ldots, N_3, \\ a^{\mathrm{kos}}, & k = N_3 + 1, \ldots, N_4, \end{cases} \tag{10}$$

to schedule the avoid-set radius across the maneuver horizon. Then the passive-safety constraints (9) can be compactly written as

$$\Gamma(t_k, x(t_k^+), a_k) = 0, \ \ \Gamma(t_k, x(t_k^-), a_k) = 0, \ \ k = 1, \ldots, N. \tag{11}$$

III. Stochastic Optimal Control Problem

This section presents the formulation of the stochastic optimal control problem for fuel-efficient rendezvous on NRHO in the presence of uncertainty. We first describe the steps required to construct the optimal control problem in the deterministic setting. In particular, we explain how time dilation is used to parametrize the impulse time instants as explicit decision variables. Then we extend the deterministic setting to account for uncertainties and formulate the stochastic optimal control problem, which models the approach-cone and passive-safety constraints as chance constraints. We also describe an approach for approximating the state distribution as Gaussian, which enables tractable reformulations of the chance constraints.

A. Time Dilation & Discretization

Since the impulse time instants $t_2, \ldots, t_N$ are decision variables, we explicitly parametrize them via time dilation. Let $\tau \in [0,1]$ be a normalized time. For each $k = 1, \ldots, N-1$, we define a dilation factor $s_k > 0$ that maps the normalized interval $[0,1]$ to the actual time interval $[t_k, t_{k+1}]$ as

$$\frac{\mathrm{d}t}{\mathrm{d}\tau} = s_k, \quad \tau \in [0,1], \tag{12}$$

with boundary conditions $t(0) = t_k$ and $t(1) = t_{k+1}$. This yields the linear mapping $t(\tau) = t_k + s_k\tau$ for $\tau \in [0,1]$. Then $s_k = t_{k+1} - t_k$, for $k = 1, \ldots, N-1$, and the total maneuver time is given by $t^{\mathrm{f}} = \sum_{k=1}^{N-1} s_k$.

Next, we use multiple shooting to parametrize a continuous-time spacecraft trajectory over the maneuver horizon with the states immediately before each impulse, denoted by x_k, for $k = 1, \ldots, N$. Let u_k denote the velocity impulse applied at time t_k. The spacecraft state immediately after the kth impulse is then given by $x_k^+ = x_k + Bu_k$, where $B = [0_{3\times 3}\ I_3]^\top$. After the kth impulse, the spacecraft trajectory satisfies the time-dilated free-drift dynamics

$$\frac{\mathrm{d}x(t(\tau))}{\mathrm{d}\tau} = s_k f(t(\tau), x(t(\tau))), \quad \tau \in [0,1]. \tag{13}$$

The state immediately before the $(k+1)$th impulse can be obtained by integrating (13) over $\tau \in [0,1]$ with initial condition x_k^+. This yields the discretized dynamics

$$x_{k+1} = F(t_k, x_k^+, s_k) \triangleq x_k^+ + \int_0^1 s_k f(t_k + s_k\tau, x(t_k + s_k\tau))\mathrm{d}\tau, \tag{14a}$$

$$t_{k+1} = t_k + s_k, \tag{14b}$$

where $x(t_k + s_k\tau)$, for $\tau \in [0,1]$, is the solution to (13) with initial condition x_k^+.

With time dilation, the isoperimetric approach-cone constraint in (6) can be expressed as

$$\Omega(t_k, x_k^+, s_k) \triangleq \int_0^1 s_k \|g^{\mathrm{ac}}(\check{r}(\tau, t_k, x_k^+, s_k))\|_+^2 \mathrm{d}\tau = 0, \quad k = 1, \ldots, N-1. \tag{15}$$

Finally, the passive-safety constraints in (11) remain unchanged under time dilation and are expressed as

$$\Gamma(t_k, x_k^+, a_k) = 0, \quad \Gamma(t_k, x_k, a_k) = 0, \quad k = 1, \ldots, N. \tag{16}$$

B. Deterministic Optimal Control Problem

In the absence of uncertainty, the fuel-efficient rendezvous maneuver can be obtained by solving an optimal control problem with constraints (14a)–(14b), (15), and (16), along with boundary conditions on time and state. However, imposing equality constraints (15) and (16) leads to a loss of linear independence constraint qualification (LICQ) at all feasible points, which is detrimental to the convergence of optimization algorithms. As a remedy, we relax the equality constraints to inequality constraints with a tolerance $\epsilon > 0$, which can be made arbitrarily small and hence without any practical impact on constraint satisfaction [42]. The resulting optimal control problem is

$$\underset{t_k, x_k, u_k, s_k}{\text{minimize}} \quad \sum_{k=1}^{N-1} \|u_k\|_2 \tag{17a}$$

$$\text{subject to} \quad x_{k+1} = F(t_k, x_k + Bu_k, s_k), \qquad k = 1, \ldots, N-1, \tag{17b}$$

$$t_{k+1} = t_k + s_k, \qquad k = 1, \ldots, N-1, \tag{17c}$$

$$s_k^{\min} \le s_k \le s_k^{\max}, \qquad k = 1, \ldots, N-1, \tag{17d}$$

$$\Omega(t_k, x_k + Bu_k, s_k) \le \epsilon, \qquad k = 1, \ldots, N-1, \tag{17e}$$

$$\Gamma(t_k, x_k, a_k) \le \epsilon, \qquad k = 1, \ldots, N, \tag{17f}$$

$$\Gamma(t_k, x_k + Bu_k, a_k) \le \epsilon, \qquad k = 1, \ldots, N, \tag{17g}$$

$$\|r_{N_j}\| \le b_j^+, \ \ r_{N_j}^\top e^{\mathrm{ac}} \ge b_j^-, \qquad j = 2, 3, \tag{17h}$$

$$x_1 = x^{\mathrm{i}}, \;\; t_1 = 0, \tag{17i}$$
$$x_N + Bu_N = x^{\mathrm{f}}, \;\; t_N \leq t^{\mathrm{f,max}}, \tag{17j}$$

where x^{i} and x^{f} are the given initial and final states, respectively. Bounds b_j^+ and b_j^-, for $j = 2, 3$, constrain the range of the spacecraft at the decision points D_2 and D_3, respectively. Bounds $s_k^{\min}$ and $s_k^{\max}$, for $k = 1, \ldots, N-1$, enforce operational limits on the impulse time instants, and $t^{\mathrm{f,max}}$ is the maximum allowable maneuver duration. When relaxing (15) and (16) to inequalities, lower-bound constraints are not required since Ω and Γ are nonnegative by construction.

C. Accounting for Uncertainty

In realistic operations, various sources of uncertainty affect the rendezvous maneuver, such as NRHO insertion error, actuation errors in the spacecraft thrusters, and navigation error (such as noise in relative range and range-rate measurements). More precisely, the initial spacecraft state, the impulses, and the estimate of the spacecraft state at each impulse time instant are all uncertain.

Let $\boldsymbol{x}^{\mathrm{i}} \sim \mathcal{N}(x^{\mathrm{i}}, \Sigma^{\mathrm{i}})$ denote the true initial state of the spacecraft at NRHO insertion. For $k = 1, \ldots, N$, let the actuation error while imparting the kth commanded impulse be modeled as a zero-mean Gaussian random vector $\boldsymbol{\mu}_k \sim \mathcal{N}(0_3, \Sigma^{\mathrm{act}})$. Let s_k, for $k = 1, \ldots, N-1$, denote the dilation factors and t_k, for $k = 1, \ldots, N$, denote the impulse time instants. We assume that there is no uncertainty in the measurement of time, i.e., the dilation factors s_k are deterministic, and as a result the impulse time instants t_k are deterministic. We assume that navigation is based on relative range and range-rate measurements. The measurement time instants are assumed to coincide with the impulse time instants. The measurement noise at time t_k, which is additive, is modeled as a zero-mean Gaussian random vector $\boldsymbol{\nu}_k \sim \mathcal{N}(0_6, \Sigma_k^{\mathrm{rr}})$. Let $\boldsymbol{x}_k$, for $k = 1, \ldots, N$, denote the true spacecraft state immediately before the kth impulse at t_k. Let $\boldsymbol{x}_k^{\mathrm{m}} = \boldsymbol{x}_k + \boldsymbol{\nu}_k$ denote the corresponding measurement of the spacecraft state. The impulse imparted at t_k consists of the (deterministic) commanded impulse u_k, a feedback component denoted by $\Lambda(\boldsymbol{x}_k^{\mathrm{m}})$, and an additive actuation error $\boldsymbol{\mu}_k$. The measured state immediately after the kth impulse is denoted by $\boldsymbol{x}_k^{\mathrm{m}+} = \boldsymbol{x}_k^{\mathrm{m}} + B(u_k + \Lambda(\boldsymbol{x}_k^{\mathrm{m}}) + \boldsymbol{\mu}_k)$.

By accounting for these uncertainties, we formulate the stochastic counterpart of (17)

$$\underset{t_k, \boldsymbol{x}_k^{\mathrm{m}}, \boldsymbol{x}_k, u_k, s_k}{\text{minimize}} \quad \sum_{k=1}^{N-1} \|u_k\|_2 \tag{18a}$$
$$\text{subject to} \quad \boldsymbol{x}_{k+1} = F(t_k, \boldsymbol{x}_k + B(u_k + \Lambda(\boldsymbol{x}_k^{\mathrm{m}}) + \boldsymbol{\mu}_k), s_k), \qquad k = 1, \ldots, N-1, \tag{18b}$$
$$t_{k+1} = t_k + s_k, \qquad k = 1, \ldots, N-1, \tag{18c}$$
$$s_k^{\min} \leq s_k \leq s_k^{\max}, \qquad k = 1, \ldots, N-1, \tag{18d}$$
$$\mathbb{P}(\Omega(t_k, \boldsymbol{x}_k^{\mathrm{m}+}, s_k) \leq \epsilon) \geq \beta^{\mathrm{ac}}, \qquad k = 1, \ldots, N-1, \tag{18e}$$
$$\mathbb{P}(\Gamma(t_k, \boldsymbol{x}_k^{\mathrm{m}}, a_k) \leq \epsilon) \geq \beta^{\mathrm{ps}}, \qquad k = 1, \ldots, N, \tag{18f}$$
$$\mathbb{P}(\Gamma(t_k, \boldsymbol{x}_k^{\mathrm{m}+}, a_k) \leq \epsilon) \geq \beta^{\mathrm{ps}}, \qquad k = 1, \ldots, N, \tag{18g}$$
$$\|\mathbb{E}(\boldsymbol{r}_{N_j})\| \leq b_j^+, \;\; \mathbb{E}(\boldsymbol{r}_{N_j})^\top e^{\mathrm{ac}} \geq b_j^-, \qquad j = 2, 3, \tag{18h}$$
$$\mathbb{E}(\boldsymbol{x}_1^{\mathrm{m}}) = x^{\mathrm{i}}, \;\; t_1 = 0, \tag{18i}$$
$$\mathbb{E}(\boldsymbol{x}_N^{\mathrm{m}+}) = x^{\mathrm{f}}, \;\; t_N \leq t^{\mathrm{f,max}}, \tag{18j}$$

where (18e)–(18g) are approach-cone and passive-safety chance constraints, respectively, with specified probability levels $\beta^{\mathrm{ac}}, \beta^{\mathrm{ps}} \in (0, 1)$. Although it is the true state of the spacecraft that must satisfy the approach-cone and passive-safety chance constraints, we do not have direct access to it due to navigation error. Therefore, we impose these chance constraints on the measured state, which is sufficient to ensure that the true state also satisfies them with the same probability levels.

Solving (18) requires a tractable characterization of the chance constraints (18e)–(18g), which in turn often requires quantifying the state distribution along the trajectory. However, since the spacecraft dynamics (1) are nonlinear, exactly propagating the state distribution is challenging in general. On the other hand, the distribution of the spacecraft state at NRHO insertion, the actuation errors, and the navigation errors throughout the maneuver are modeled as Gaussian. Therefore, when the spacecraft dynamics are linearized about a reference

solution, the state distribution across the maneuver horizon can be approximated as Gaussian, and hence fully characterized by its mean and covariance.

To that end, let $\bar{t}_k, \bar{x}_k, \bar{u}_k$, for $k = 1, \ldots, N$, and $\bar{s}_k$ for $k = 1, \ldots, N-1$, denote a reference solution. Let the evaluation of F and its gradients at the reference solution be denoted as

$$\begin{aligned}
\bar{F}_k &= F(\bar{t}_k, \bar{x}_k + B\bar{u}_k, \bar{s}_k), && k = 1, \ldots, N-1, && \text{(19a)}\\
T_k &= \nabla_1 F(\bar{t}_k, \bar{x}_k + B\bar{u}_k, \bar{s}_k), && k = 1, \ldots, N-1, && \text{(19b)}\\
A_k &= \nabla_2 F(\bar{t}_k, \bar{x}_k + B\bar{u}_k, \bar{s}_k), && k = 1, \ldots, N-1, && \text{(19c)}\\
S_k &= \nabla_3 F(\bar{t}_k, \bar{x}_k + B\bar{u}_k, \bar{s}_k), && k = 1, \ldots, N-1, && \text{(19d)}\\
w_k &= \bar{F}_k - T_k\bar{t}_k - A_k(\bar{x}_k + B\bar{u}_k) - S_k\bar{s}_k, && k = 1, \ldots, N-1. && \text{(19e)}
\end{aligned}$$

Using the reference solution and the gradients defined above, we obtain a linearized approximation of the dynamics of the spacecraft states immediately before each impulse as

$$\begin{aligned}
\boldsymbol{x}_{k+1} &= T_k t_k + A_k \boldsymbol{x}_k + A_k B(u_k + \boldsymbol{\mu}_k) + S_k s_k + w_k, \;\; k = 1, \ldots, N-1, && \text{(20a)}\\
\boldsymbol{x}_1 &= \boldsymbol{x}^{\mathrm{i}}, && \text{(20b)}
\end{aligned}$$

where we ignore the feedback component for now, and incorporate it later once the dynamics of the measured state are introduced. Since the initial state and actuation errors are modeled as Gaussian, the linearity of (20a) ensures that $\boldsymbol{x}_k$ is also Gaussian for each $k = 1, \ldots, N$. Let x_k, for $k = 1, \ldots, N$, denote the mean spacecraft state immediately before each impulse, which satisfies

$$\begin{aligned}
x_{k+1} &= T_k t_k + A_k x_k + A_k B u_k + S_k s_k + w_k, \;\; k = 1, \ldots, N-1, && \text{(21a)}\\
x_1 &= x^{\mathrm{i}}. && \text{(21b)}
\end{aligned}$$

Due to the presence of navigation error, we do not have direct access to $\boldsymbol{x}_k$. Instead, we obtain a measurement $\boldsymbol{x}_k^{\mathrm{m}} = \boldsymbol{x}_k + \boldsymbol{\nu}_k$. Then the measured spacecraft state immediately before each impulse satisfies

$$\begin{aligned}
\boldsymbol{x}_{k+1}^{\mathrm{m}} &= T_k t_k + A_k \boldsymbol{x}_k^{\mathrm{m}} + A_k B(u_k + \boldsymbol{\mu}_k) + S_k s_k + w_k + \boldsymbol{\nu}_{k+1} - A_k \boldsymbol{\nu}_k, \;\; k = 1, \ldots, N-1, && \text{(22a)}\\
\boldsymbol{x}_1^{\mathrm{m}} &= \boldsymbol{x}^{\mathrm{i}} + \boldsymbol{\nu}_1. && \text{(22b)}
\end{aligned}$$

For $k = 1, \ldots, N$, the measured spacecraft states $\boldsymbol{x}_k^{\mathrm{m}}$ are also Gaussian with mean x_k (satisfying (21a)–(21b)) and covariance denoted by Σ_k^{m}. However, in the absence of a feedback mechanism, the covariance of the measured states can grow unbounded over time, which can lead to overly conservative chance constraints. To mitigate this issue, we introduce a stabilizing feedback law based on the Fixed-Time-of-Arrival (FTA) approach, which has significant flight heritage. Specifically, we modify (22a) to include an affine feedback term $\Lambda(\boldsymbol{x}_k^{\mathrm{m}}) = K_k(\boldsymbol{x}_k^{\mathrm{m}} - x_k)$ added to the commanded impulse u_k, with gain $K_k \in \mathbb{R}^{3\times 6}$ given by

$$K_k = -(RA_kB)^{-1}RA_k, \tag{23}$$

with $R = [I_3 \; 0_{3\times 3}]$. Such a feedback mechanism greedily drives the spacecraft position to the reference position at the next impulse time instant in the absence of actuation and navigation errors. The measured state immediately after the kth impulse is given by

$$\boldsymbol{x}_k^{\mathrm{m}+} = \boldsymbol{x}_k^{\mathrm{m}} + B(u_k + K_k(\boldsymbol{x}_k^{\mathrm{m}} - x_k) + \boldsymbol{\mu}_k), \;\; k = 1, \ldots, N. \tag{24}$$

The linearized closed-loop dynamics of the measured spacecraft states immediately before each impulse are

$$\begin{aligned}
\boldsymbol{x}_{k+1}^{\mathrm{m}} &= T_k t_k + (A_k + A_kBK_k)\boldsymbol{x}_k^{\mathrm{m}} + A_kB(u_k - K_k x_k + \boldsymbol{\mu}_k) + S_k s_k + w_k + \boldsymbol{\nu}_{k+1} - A_k\boldsymbol{\nu}_k, \;\; k = 1, \ldots, N-1, && \text{(25a)}\\
\boldsymbol{x}_1^{\mathrm{m}} &= \boldsymbol{x}^{\mathrm{i}} + \boldsymbol{\nu}_1. && \text{(25b)}
\end{aligned}$$

Then, the covariance of the measured spacecraft states immediately before each impulse satisfies

$$\begin{aligned}
\Sigma_{k+1}^{\mathrm{m}} &= (A_k + A_kBK_k)\Sigma_k^{\mathrm{m}}(A_k + A_kBK_k)^\top + A_kB\Sigma^{\mathrm{act}}B^\top A_k^\top + \Sigma_{k+1}^{\mathrm{rr}} + A_k\Sigma_k^{\mathrm{rr}}A_k^\top, \;\; k = 1, \ldots, N-1, && \text{(26a)}\\
\Sigma_1^{\mathrm{m}} &= \Sigma^{\mathrm{i}} + \Sigma_1^{\mathrm{rr}}. && \text{(26b)}
\end{aligned}$$

IV. Sequential Convex Programming Solution Approach

This section presents the sequential convex programming (SCP) solution approach to solve the stochastic optimal control problem (18). We first obtain deterministic reformulations for the chance constraints and then present the SCP algorithm that uses these reformulations.

A. Deterministic Reformulation of Chance Constraints

We now derive deterministic reformulations for the chance constraints (18e)–(18g). As with the dynamics, we linearize the approach-cone and passive-safety constraints about a reference solution to obtain tractable approximations. Specifically, let $\bar{t}_k, \bar{x}_k, \bar{u}_k$, for $k = 1, \ldots, N$, and $\bar{s}_k$ for $k = 1, \ldots, N-1$, denote the reference solution. Let the evaluation of Ω and Γ and their gradients at the reference solution be denoted as

$$
\begin{aligned}
\bar{\Omega}_k &= \Omega(\bar{t}_k, \bar{x}_k + B\bar{u}_k, \bar{s}_k), && k = 1, \ldots, N-1, && \text{(27a)}\\
G_{n,k} &= \nabla_n \Omega(\bar{t}_k, \bar{x}_k + B\bar{u}_k, \bar{s}_k), && k = 1, \ldots, N-1, \;\; n = 1,2,3, && \text{(27b)}\\
g_k &= \bar{\Omega}_k - G_{1,k}\bar{t}_k - G_{2,k}(\bar{x}_k + B\bar{u}_k) - G_{3,k}\bar{s}_k, && k = 1, \ldots, N-1, && \text{(27c)}\\
\bar{\Gamma}_k^- &= \Gamma(\bar{t}_k, \bar{x}_k, a_k), && k = 1, \ldots, N, && \text{(27d)}\\
H_{n,k}^- &= \nabla_n \Gamma(\bar{t}_k, \bar{x}_k, a_k), && k = 1, \ldots, N, \;\; n = 1,2, && \text{(27e)}\\
h_k^- &= \bar{\Gamma}_k^- - H_{1,k}^- \bar{t}_k - H_{2,k}^- \bar{x}_k, && k = 1, \ldots, N, && \text{(27f)}\\
\bar{\Gamma}_k^+ &= \Gamma(\bar{t}_k, \bar{x}_k + B\bar{u}_k, a_k), && k = 1, \ldots, N, && \text{(27g)}\\
H_{n,k}^+ &= \nabla_n \Gamma(\bar{t}_k, \bar{x}_k + B\bar{u}_k, a_k), && k = 1, \ldots, N, \;\; n = 1,2, && \text{(27h)}\\
h_k^+ &= \bar{\Gamma}_k^+ - H_{1,k}^+ \bar{t}_k - H_{2,k}^+ (\bar{x}_k + B\bar{u}_k), && k = 1, \ldots, N, && \text{(27i)}
\end{aligned}
$$

where Ω and Γ are differentiable functions, and the computation of their gradients is detailed in Appendix A. The chance constraints (18e)–(18g) can be approximated using linearizations of the approach-cone and passive-safety constraints as

$$
\begin{aligned}
&\mathbb{P}(G_{1,k}t_k + G_{2,k}\boldsymbol{x}_k^{\mathrm{m}+} + G_{3,k}s_k + g_k \le \epsilon) \ge \beta^{\mathrm{ac}}, && k = 1, \ldots, N-1, && \text{(28a)}\\
&\mathbb{P}(H_{1,k}^- t_k + H_{2,k}^- \boldsymbol{x}_k^{\mathrm{m}} + h_k^- \le \epsilon) \ge \beta^{\mathrm{ps}}, && k = 1, \ldots, N, && \text{(28b)}\\
&\mathbb{P}(H_{1,k}^+ t_k + H_{2,k}^+ \boldsymbol{x}_k^{\mathrm{m}+} + h_k^+ \le \epsilon) \ge \beta^{\mathrm{ps}}, && k = 1, \ldots, N. && \text{(28c)}
\end{aligned}
$$

We now leverage a widely used deterministic reformulation for chance constraints of the form $\mathbb{P}(a^\top \boldsymbol{z} \le b) \ge \beta$, where $\boldsymbol{z} \sim \mathcal{N}(\mu^z, \Sigma^z)$, $\beta \in (0,1)$ is the specified probability level, and $a \in \mathbb{R}^n$, $b \in \mathbb{R}$ are known,

$$
a^\top \mu^z + \sqrt{Q_n(\beta) a^\top \Sigma^z a} \le b \implies \mathbb{P}(a^\top \boldsymbol{z} \le b) \ge \beta, \tag{29}
$$

where $Q_n(\beta)$ is the quantile function of a chi-squared distribution with n degrees of freedom. Then satisfaction of the following deterministic constraints implies satisfaction of the chance constraints (28):

$$
\begin{aligned}
&G_{1,k}t_k + G_{2,k}(x_k + Bu_k) + G_{3,k}s_k + g_k + \sqrt{Q_6(\beta^{\mathrm{ac}}) G_{2,k}\Sigma_k^{\mathrm{m}} G_{2,k}^\top} \le \epsilon, && k = 1, \ldots, N-1, && \text{(30a)}\\
&H_{1,k}^- t_k + H_{2,k}^- x_k + h_k^- + \sqrt{Q_6(\beta^{\mathrm{ps}}) H_{2,k}^- \Sigma_k^{\mathrm{m}} (H_{2,k}^-)^\top} \le \epsilon, && k = 1, \ldots, N, && \text{(30b)}\\
&H_{1,k}^+ t_k + H_{2,k}^+ (x_k + Bu_k) + h_k^+ + \sqrt{Q_6(\beta^{\mathrm{ps}}) H_{2,k}^+ \Sigma_k^{\mathrm{m}} (H_{2,k}^+)^\top} \le \epsilon, && k = 1, \ldots, N. && \text{(30c)}
\end{aligned}
$$

For convenience of notation, we define

$$
\begin{aligned}
\bar{g}_k &\triangleq g_k + \sqrt{Q_6(\beta^{\mathrm{ac}}) G_{2,k}\Sigma_k^{\mathrm{m}} G_{2,k}^\top}, && k = 1, \ldots, N-1, && \text{(31a)}\\
\bar{h}_k^- &\triangleq h_k^- + \sqrt{Q_6(\beta^{\mathrm{ps}}) H_{2,k}^- \Sigma_k^{\mathrm{m}} (H_{2,k}^-)^\top}, && k = 1, \ldots, N, && \text{(31b)}\\
\bar{h}_k^+ &\triangleq h_k^+ + \sqrt{Q_6(\beta^{\mathrm{ps}}) H_{2,k}^+ \Sigma_k^{\mathrm{m}} (H_{2,k}^+)^\top}, && k = 1, \ldots, N. && \text{(31c)}
\end{aligned}
$$

The reformulated constraints (30a)–(30c) are approximate, due to the linearizations with respect to an arbitrary reference solution. However, by iteratively updating the reference solution, we can obtain increasingly accurate approximations, which is a key feature of the solution approach described next.

B. Sequential Convex Programming

Sequential convex programming (SCP) algorithms are widely used for solving optimal control problems. They consist of iteratively solving convex subproblems obtained by linearizing and exactly penalizing the nonconvex constraints (typically about the solution of the subproblem from the previous SCP iterate), and by penalizing deviations from the previous iterate in the objective function. The application of SCP to solve (18) involves certain subtleties due to the presence of chance constraints. We treat (i) the impulse time instants t_k, for $k = 1, \ldots, N$, (ii) the mean spacecraft state immediately before each impulse x_k, for $k = 1, \ldots, N$, (iii) the commanded impulses u_k, for $k = 1, \ldots, N$, and (iv) the dilation factors s_k, for $k = 1, \ldots, N-1$, as the decision variables of the subproblem. We use the previous SCP iterate as the reference solution to obtain the linearized dynamics constraint (21a), the reformulated chance constraints (30a)–(30c), and the covariance of the measured spacecraft states (26a)–(26b) (which also requires recomputation of the FTA feedback gains in (23)). These constraints are exactly penalized in the subproblem objective function using an ℓ_1-norm penalty. The boundary conditions (18i) and (18j) are imposed on the mean spacecraft state, since the expected value of the measured state is equal to the mean state.

At an arbitrary SCP iterate, let $\bar{t}_k, \bar{x}_k, \bar{u}_k$, for $k = 1, \ldots, N$, and $\bar{s}_k$ for $k = 1, \ldots, N-1$, denote the reference solution, i.e., the solution of the previous SCP iterate. The SCP subproblem is formulated as

$$
\begin{aligned}
\underset{t_k, x_k, u_k, s_k}{\text{minimize}} \quad & \sum_{k=1}^{N-1} \|u_k\|_2 + \frac{w^{\text{px}}}{2} \sum_{k=1}^{N} (\|x_k - \bar{x}_k\|^2 + \|u_k - \bar{u}_k\|^2) && && \text{(32a)} \\
& + \frac{w^{\text{px}}}{2}(t_N - \bar{t}_N)^2 + \frac{w^{\text{px}}}{2} \sum_{k=1}^{N-1} ((t_k - \bar{t}_k)^2 + (s_k - \bar{s}_k)^2) \\
& + w^{\text{ep}} \sum_{k=1}^{N-1} \|x_{k+1} - T_k t_k - A_k(x_k + Bu_k) - S_k s_k - w_k\|_1 \\
& + w^{\text{ep}} \sum_{k=1}^{N-1} |G_{1,k} t_k + G_{2,k}(x_k + Bu_k) + G_{3,k} s_k + \bar{g}_k - \epsilon|_+ \\
& + w^{\text{ep}} \sum_{k=1}^{N} |H^-_{1,k} t_k + H^-_{2,k} x_k + \bar{h}^-_k - \epsilon|_+ \\
& + w^{\text{ep}} \sum_{k=1}^{N} |H^+_{1,k} t_k + H^+_{2,k}(x_k + Bu_k) + \bar{h}^+_k - \epsilon|_+ \\
\text{subject to} \quad & t_{k+1} = t_k + s_k, && k = 1, \ldots, N-1, && \text{(32b)} \\
& s^{\min}_k \le s_k \le s^{\max}_k, && k = 1, \ldots, N-1, && \text{(32c)} \\
& \|r_{N_j}\| \le b^+_j, \;\; r_{N_j}^\top e^{\text{ac}} \ge b^-_j, && j = 2, 3, && \text{(32d)} \\
& x_1 = x^{\text{i}}, \;\; t_1 = 0, && && \text{(32e)} \\
& x_N + Bu_N = x^{\text{f}}, \;\; t_N \le t^{\text{f,max}}, && && \text{(32f)}
\end{aligned}
$$

where $w^{\text{px}} > 0$ and $w^{\text{ep}} > 0$ are the weights for the proximal term (penalizing deviation from the previous iterate) and the exact penalty terms, respectively. These weights can be adaptively tuned in conjunction with line searches to ensure guaranteed convergence of SCP, i.e., $t_k \to \bar{t}_k$, $x_k \to \bar{x}_k$, $u_k \to \bar{u}_k$, for $k = 1, \ldots, N$, and $s_k \to \bar{s}_k$, for $k = 1, \ldots, N-1$, as the SCP iterates progress. The convergence of the SCP algorithm is assessed using the following termination criteria: (i) the maximum change in decision variables across successive iterates is below a specified tolerance, and (ii) the maximum constraint violation across the exact penalty terms is below a specified tolerance. The components of the SCP algorithm are illustrated as a block diagram in Figure 2. Note that, at convergence, the linearized dynamics constraint (21a) and the reformulated chance constraints (30a)–(30c) are equivalent to

$$
\begin{aligned}
& x_{k+1} = F(t_k, x_k + Bu_k, s_k), && k = 1, \ldots, N-1, && \text{(33a)} \\
& \Omega(t_k, x_k + Bu_k, s_k) + \sqrt{Q_6(\beta^{\text{ac}}) G_{2,k} \Sigma^{\text{m}}_k G_{2,k}^\top} \le \epsilon, && k = 1, \ldots, N-1, && \text{(33b)} \\
& \Gamma(t_k, x_k, a_k) + \sqrt{Q_6(\beta^{\text{ps}}) H^-_{2,k} \Sigma^{\text{m}}_k (H^-_{2,k})^\top} \le \epsilon, && k = 1, \ldots, N, && \text{(33c)} \\
& \Gamma(t_k, x_k + Bu_k, a_k) + \sqrt{Q_6(\beta^{\text{ps}}) H^+_{2,k} \Sigma^{\text{m}}_k (H^+_{2,k})^\top} \le \epsilon, && k = 1, \ldots, N.. && \text{(33d)}
\end{aligned}
$$

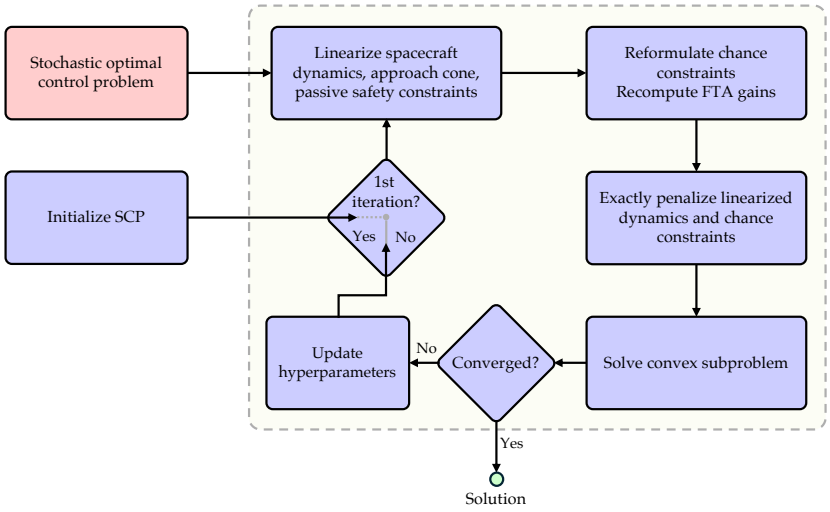

Fig. 2 Block diagram of the sequential convex programming solution approach for solving the stochastic optimal control problem (18).

In other words, at convergence, the expected values of the true and measured spacecraft states immediately before each impulse satisfy the actual nonlinear dynamics of the spacecraft (14a). The expected values of the measured spacecraft states before the impulse satisfy the approach-cone constraints (15) with a safety margin, and the expected values of the measured spacecraft states before and after the impulse satisfy the passive-safety constraints (16) with a safety margin. The safety margins in (33b)–(33d) approximately correspond to the β^{ac} and β^{ps} confidence sets of the measured spacecraft states. A β confidence set of a random variable is the set containing the realizations of the random variable with probability β.

V. Numerical Results

This section demonstrates the proposed SCP-based approach through a numerical case study of spacecraft rendezvous with the Gateway, using the specifications in Section II.A. The parameter values are listed in Table 2 and include: (i) the number of nodes in the time grid for each phase; (ii) bounds on the time between successive thruster firings; (iii) the covariances of the spacecraft state at NRHO insertion, the relative-range measurements at the decision points, and the actuation error; (iv) chance-constraint confidence levels; (v) parameters of the approach-cone constraint and the range constraints at D_2 and D_3; and (vi) the initial and final values of the mean spacecraft state. These values are based on related case studies in [44]. The initial and final positions, as well as the approach-cone axis, are specified in the Sun-Referenced LVLH frame. We use the rotation matrix T^{LVLH} to transform position and velocity from the Sun-Referenced LVLH frame to the Gateway-centered inertial frame used in the dynamical model (1). The matrix ${}^{r}E$ in Table 2 selects the position components from the state vector.

At far range (near D_1), the spacecraft relies on ground-based orbit determination; at mid range (beyond D_2), it uses line-of-sight (LOS) and Gateway-relative measurements. Accordingly, we specify the covariance of the relative-range measurements at the decision points and linearly interpolate these values between successive decision points. This simplification is physically reasonable because the range decreases roughly monotonically from D_1 to D_4, and it preserves tractability of the SCP formulation and the chance-constraint representation. The bounds on the time between successive thruster firings, $s_k^{\min}$ and $s_k^{\max}$ for $k = 1, \ldots, N-1$, are chosen to balance operational limits on thruster firing frequency with the time required for the spacecraft to traverse each phase.

We initialize the state with a straight-line profile by linearly interpolating the boundary conditions at D_1 and D_4 across the intermediate nodes, and we set the control input to zero. We use two layers of scaling within the SCP algorithm to ensure reliable numerical performance. First, we scale the continuous-time dynamics (1)

by choosing physically meaningful units (hr, km, km/hr) so that the state and control profiles have similar magnitudes [31]. Second, after constructing the convex subproblem (32), we apply an affine scaling to the decision variables to ensure comparable orders of magnitude and precondition the constraint matrices via row normalization [33], which improves SCP convergence [45]. After scaling and preconditioning, choosing ϵ in (17e)–(17g) on the order of 10^{-3}–10^{-4} yields no physically meaningful violations of the original (unrelaxed) constraints.

We performed a 1000-sample Monte Carlo simulation using a rendezvous maneuver computed via the proposed method. Table 1 summarizes fuel consumption and constraint satisfaction across the samples. Notably, none of the samples violate the passive-safety constraint. This behavior reflects the conservativeness of the chance-constraint reformulation described in Section IV.A: even relatively small values of β^{ps} (e.g., around 0.8) can yield a high percentage of safe outcomes in Monte Carlo simulations. For a detailed discussion of the conservativeness of chance-constraint formulations, we refer the reader to [46].

The computed rendezvous maneuver and the Monte Carlo simulation are visualized as follows. Figure 3 displays the position trajectories of the Monte Carlo samples in the Sun-Referenced LVLH frame (coordinates r_1, r_2, r_3), where blue curves denote samples and black curves denote the mean trajectory; dots indicate discretization nodes. The avoid sets for the three phases are shown in red. The spacecraft follows a roundabout path to the Gateway to maintain passive safety. Figure 4 presents histograms of the closed-loop impulse magnitudes across the three-phase maneuver, denoted as Δv_k, for $k = 1, \ldots, N$. The first three rows show phase-wise histograms of impulse magnitudes, and the fourth row shows the histogram of total fuel consumption (Δv).

Table 1 Fuel consumption and constraint satisfaction in 1000-sample Monte Carlo simulation

Statistic	**Value**
Mean / Minimum / Maximum fuel consumption	18.5 / 13.3 / 25.9 m/s
Samples violating passive-safety constraint	0 %
Samples violating approach-cone constraint	0.5 %

The proposed approach is more fuel-efficient than our prior work [13] because it optimizes the impulse time instants. However, it does not guarantee underburn safety, which we do not evaluate in this case study. Direct comparison of fuel-consumption statistics with other NRHO rendezvous methods is difficult because published simulations use different key parameters (Table 2), particularly the spacecraft state at NRHO insertion [14–18, 44]. Nonetheless, our method achieves fuel consumption in a comparable range while uniquely ensuring continuous-time satisfaction of the passive-safety and approach-cone path chance constraints.

Table 2 Parameter values for the three-phase rendezvous maneuver to the Gateway

Parameter	Value
N_2, N_3, N	4, 8, 12
r^{rs}, r^{as}, r^{kos} [km]	10, 1, 0.2
t^{s} [hr]	24
$t^{\mathrm{f,max}}$ [hr]	48
s_k^{min} [hr]	30, 8, 2, 0.1, 0.1, 0.1, 0.1, 0.1, 0.1, 0.1, 0.1
s_k^{max} [hr]	35, 15, 5, 3, 3, 3, 3, 3, 3, 3, 3
Σ^{i} [$\mathrm{km}^2, \mathrm{km}^2/\mathrm{hr}^2$]	$\mathrm{blkdiag}(33.33I_3, 6I_3)^2$
Σ_1^{rr} [$\mathrm{km}^2, \mathrm{km}^2/\mathrm{hr}^2$]	$\mathrm{blkdiag}(6.66I_3, 0.25I_3)^2$
$\Sigma_{N_2}^{\mathrm{rr}}$ [$\mathrm{km}^2, \mathrm{km}^2/\mathrm{hr}^2$]	$\mathrm{blkdiag}(0.08I_3, 0.04I_3)^2$
$\Sigma_{N_3}^{\mathrm{rr}}$ [$\mathrm{km}^2, \mathrm{km}^2/\mathrm{hr}^2$]	$\mathrm{blkdiag}(0.009I_3, 0.03I_3)^2$
Σ_N^{rr} [$\mathrm{km}^2, \mathrm{km}^2/\mathrm{hr}^2$]	$\mathrm{blkdiag}(0.006I_3, 0.01I_3)^2$
Σ^{act} [$\mathrm{km}^2/\mathrm{hr}^2$]	$10^{-3}I_3^2$
β^{ps}, β^{ac}	0.8, 0.8
θ^{ac}, e^{ac}	55°, ${}^{T^{\mathrm{LVLH}}}E^{\top}(0,0,1)$
x^{i}, x^{f} [km, km/hr]	$T^{\mathrm{LVLH}}(0,-600,800,2.5,30,-20)$, $T^{\mathrm{LVLH}}(0,0,0.5,0,0,0)$
b_2^+, b_2^-, b_3^+, b_3^- [km]	55, 45, 6.5, 3.5

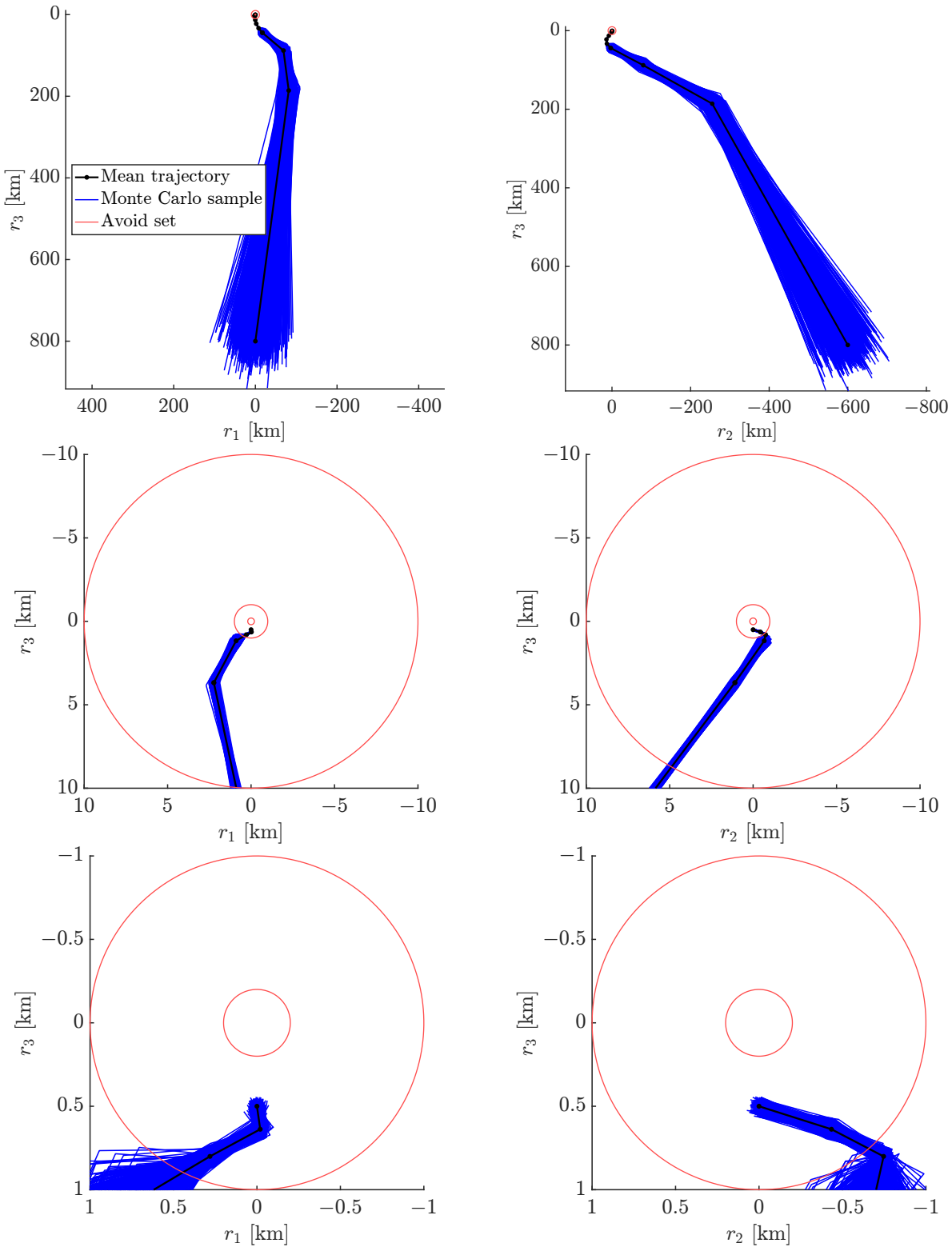

Fig. 3 Monte Carlo simulation of the NRHO rendezvous maneuver.

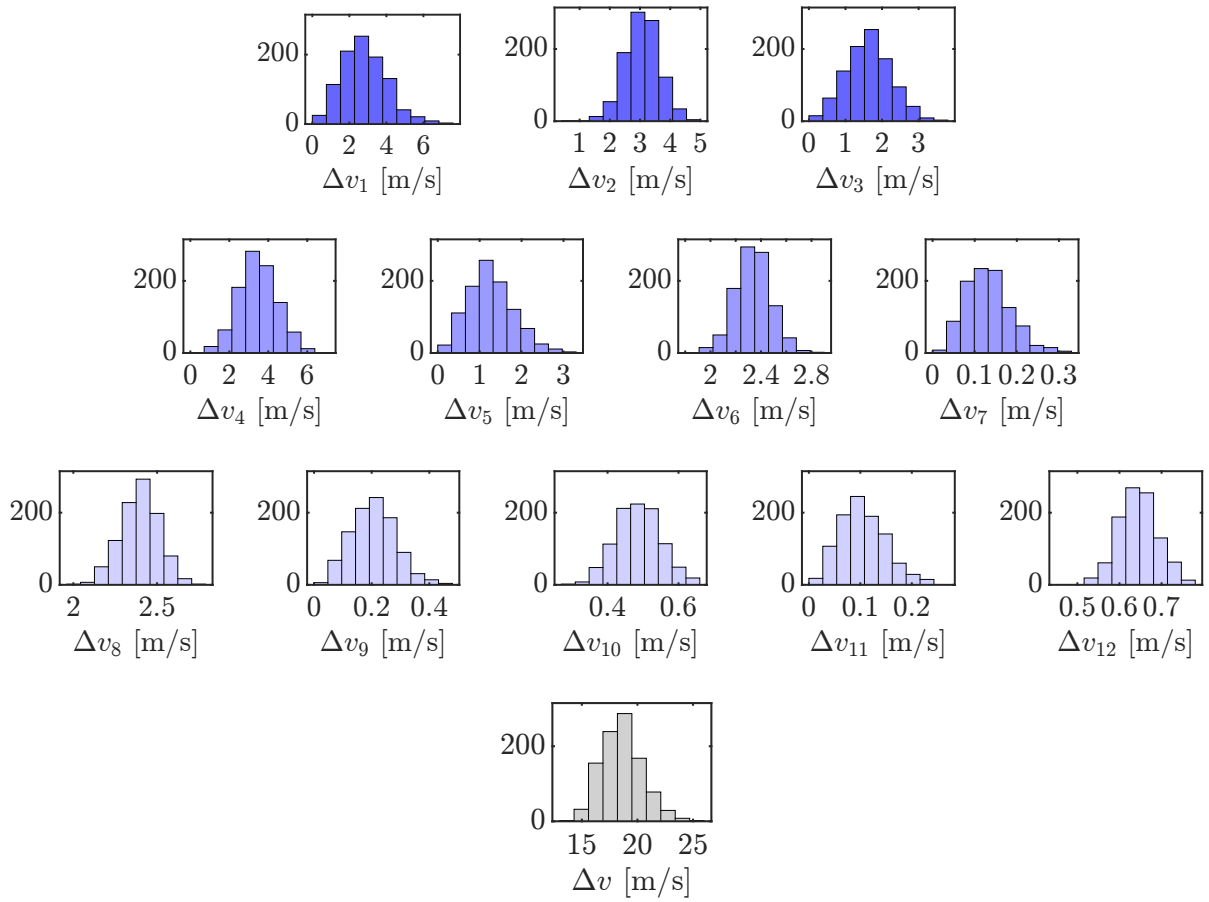

Fig. 4 Monte Carlo simulation of closed-loop control input magnitudes and total fuel consumption across the three-phase rendezvous maneuver.

VI. Conclusion

We proposed a method for safe, fuel-efficient spacecraft rendezvous with the Gateway using sequential convex programming. The approach (i) enforces passive safety at all times and satisfies the approach-cone path constraint in continuous time; (ii) meets the requirements for decision points along the rendezvous trajectory in accordance with IRSIS guidelines; and (iii) models uncertainties from NRHO insertion, actuation errors, and navigation measurements via chance constraints while employing a stabilizing feedback mechanism to bound the dispersions. To prevent inter-sample violations that may occur when constraints are imposed only at time nodes, we reformulated the continuous-time path constraints as integral constraints via an isoperimetric construction. We demonstrated the method on a realistic Gateway rendezvous case study and validated it through Monte Carlo simulations. The results confirmed that the probabilistic constraints (passive-safety and approach-cone) were satisfied with sufficiently high probability, and achieved a fuel consumption comparable to those reported in recent NRHO rendezvous studies.

A. Gradient of Ω and Γ

The gradient of Γ (in constraint (16)) with respect to the first and second arguments and evaluated at t_k, x_k, a_k for some $k = 1, \dots, N$ is given by

$$\nabla_n \Gamma(t_k, x_k, a_k) = -4 \int_0^{t^s} \|a_k^2 - \|\check{r}(\gamma, t_k, x_k, t^s)\|^2\|_+ \|\check{r}(\gamma, t_k, x_k, t^s)\| \nabla_{n+1} \check{r}(\gamma, t_k, x_k, t^s) \mathrm{d}\gamma, \quad n = 1, 2, \tag{34}$$

where $\nabla_{n+1}\check{r}(\gamma, t_k, x_k, t^s)$ is the sensitivity of the position along the free-drift trajectory with respect to changes in initial time (t_k), for $n = 1$, and initial state (x_k), for $n = 2$. These sensitivities can be computed by solving the initial-value problem

$$\begin{aligned}
\frac{\mathrm{d}}{\mathrm{d}\gamma} \nabla_2 \check{x}(\gamma, t_k, x_k, t^s) &= \nabla_1 f(t_k + \gamma, \check{x}(\gamma, t_k, x_k, t^s)) + \nabla_2 f(t_k + \gamma, \check{x}(\gamma, t_k, x_k, t^s)) \nabla_2 \check{x}(\gamma, t_k, x_k, t^s), \quad \gamma \in [0, t^s], \\
\nabla_2 \check{x}(0, t_k, x_k, t^s) &= 0_6, \\
\frac{\mathrm{d}}{\mathrm{d}\gamma} \nabla_3 \check{x}(\gamma, t_k, x_k, t^s) &= \nabla_2 f(t_k + \gamma, \check{x}(\gamma, t_k, x_k, t^s)) \nabla_3 \check{x}(\gamma, t_k, x_k, t^s), \qquad \gamma \in [0, t^s], \\
\nabla_3 \check{x}(0, t_k, x_k, t^s) &= I_6,
\end{aligned}$$

where the first three rows of $\nabla_n \check{x}(\gamma, t_k, x_k, t^s)$ yield $\nabla_n \check{r}(\gamma, t_k, x_k, t^s)$ for $n = 2, 3$.

The gradient of Ω (in (15)) evaluated at t_k, x_k^+, s_k for some $k = 1, \dots, N-1$ is given by

$$\nabla_1 \Omega(t_k, x_k^+, s_k) = 2 \int_0^1 s_k \|g^{\mathrm{ac}}(\check{r}(\tau, t_k, x_k^+, s_k))\|_+^2 \nabla g^{\mathrm{ac}}(\check{r}(\tau, t_k, x_k^+, s_k)) \nabla_2 \check{r}(\tau, t_k, x_k^+, s_k) \mathrm{d}\tau, \tag{35a}$$

$$\nabla_2 \Omega(t_k, x_k^+, s_k) = 2 \int_0^1 s_k \|g^{\mathrm{ac}}(\check{r}(\tau, t_k, x_k^+, s_k))\|_+^2 \nabla g^{\mathrm{ac}}(\check{r}(\tau, t_k, x_k^+, s_k)) \nabla_3 \check{r}(\tau, t_k, x_k^+, s_k) \mathrm{d}\tau, \tag{35b}$$

$$\begin{aligned}
\nabla_3 \Omega(t_k, x_k^+, s_k) = 2 \int_0^1 & s_k \|g^{\mathrm{ac}}(\check{r}(\tau, t_k, x_k^+, s_k))\|_+^2 \nabla g^{\mathrm{ac}}(\check{r}(\tau, t_k, x_k^+, s_k)) \nabla_4 \check{r}(\tau, t_k, x_k^+, s_k) \mathrm{d}\tau \\
& + \int_0^1 \|g^{\mathrm{ac}}(\check{r}(\tau, t_k, x_k^+, s_k))\|_+^2 \mathrm{d}\tau,
\end{aligned} \tag{35c}$$

where $\nabla_{n+1}\check{r}(\tau, t_k, x_k^+)$ is the sensitivity of the position along the free-drift trajectory with respect to changes in initial time (t_k), for $n = 1$, initial state (x_k^+), for $n = 2$, and time-interval length (i.e., dilation factor s_k), for $n = 3$. These sensitivities can be computed by solving the initial-value problem

$$\begin{aligned}
\frac{\mathrm{d}}{\mathrm{d}\tau} \nabla_2 \check{x}(\tau, t_k, x_k^+, s_k) &= s_k \nabla_2 f(t_k + s_k\tau, \check{x}(\tau, t_k, x_k^+, s_k)) \nabla_2 \check{x}(\tau, t_k, x_k^+, s_k) \qquad \tau \in [0, 1], \\
&\quad + s_k \nabla_1 f(t_k + s_k\tau, \check{x}(\tau, t_k, x_k^+, s_k)), \\
\nabla_2 \check{x}(0, t_k, x_k^+, s_k) &= 0_6, \\
\frac{\mathrm{d}}{\mathrm{d}\tau} \nabla_3 \check{x}(\tau, t_k, x_k^+, s_k) &= s_k \nabla_2 f(t_k + s_k\tau, \check{x}(\tau, t_k, x_k^+, s_k)) \nabla_3 \check{x}(\tau, t_k, x_k^+, s_k), \qquad \tau \in [0, 1], \\
\nabla_3 \check{x}(0, t_k, x_k^+, s_k) &= I_6,
\end{aligned}$$

$$\begin{aligned}\frac{\mathrm{d}}{\mathrm{d}\tau}\nabla_4\check{x}(\tau,t_k,x_k^+,s_k) &= s_k\nabla_2 f(t_k+s_k\tau,\check{x}(\tau,t_k,x_k^+,s_k))\nabla_4\check{x}(\tau,t_k,x_k^+,s_k) && \tau\in[0,1],\\ &\quad + s_k\tau\nabla_1 f(t_k+s_k\tau,\check{x}(\tau,t_k,x_k^+,s_k)) + f(t_k+s_k\tau,\check{x}(\tau,t_k,x_k^+,s_k)),\\ \nabla_4\check{x}(0,t_k,x_k^+,s_k) &= 0_6\end{aligned}$$

References

[1] Fuller, S., Lehnhardt, E., Olansen, J., Mason, J. S., Connell, D., Travis, T., and Fleming, C., "Gateway Program Development Progress," *75th International Astronautical Congress (IAC)*, International Astronautical Federation (IAF), 2024, pp. 1–6.

[2] Lee, D. E., "Gateway destination orbit model: a continuous 15 year NRHO reference trajectory," Tech. rep., NASA Johnson Space Center Houston, TX, 2019.

[3] Flores-Abad, A., Ma, O., Pham, K., and Ulrich, S., "A review of space robotics technologies for on-orbit servicing," *Progress in Aerospace Sciences*, Vol. 68, 2014, pp. 1–26. https://doi.org/10.1016/j.paerosci.2014.03.002.

[4] Ueda, S., Ikenaga, T., Maeda, M., Yamamoto, T., and Ikeda, H., "Practical rendezvous scenario for transportation missions to cis-lunar station in earth-moon L2 halo orbit," *Proceedings of the 25th International Symposium on Space Flight Dynamics (ISSFD)*, 2015, pp. 1–24.

[5] NASA, ROSCOMOS, JAXA, ESA, and CSA, "International Rendezvous System Interoperability Standards (IRSIS)," Tech. rep., NASA, ESA, CSA, JAXA, ROSCOSMOS, Mar. 2019. URL https://internationaldeepspacestandards.com/.

[6] Marsillach, D. A., Di Cairano, S., and Weiss, A., "Fail-safe Rendezvous Control on Elliptic Orbits using Reachable Sets," *2020 American Control Conference (ACC)*, IEEE, 2020, pp. 4920–4925. https://doi.org/10.23919/acc45564.2020.9147957.

[7] Bucci, L., Colagrossi, A., and Lavagna, M., "Rendezvous in Lunar Near Rectilinear Halo Orbits," *Advances in Astronautics Science and Technology*, Vol. 1, No. 1, 2018, pp. 39–43. https://doi.org/10.1007/s42423-018-0012-6.

[8] Lizy-Destrez, S., Beauregard, L., Blazquez, E., Campolo, A., Manglativi, S., and Quet, V., "Rendezvous Strategies in the Vicinity of Earth-Moon Lagrangian Points," *Frontiers in Astronomy and Space Sciences*, Vol. 5, 2019. https://doi.org/10.3389/fspas.2018.00045.

[9] Blazquez, E., Beauregard, L., Lizy-Destrez, S., Ankersen, F., and Capolupo, F., "Rendezvous design in a cislunar near rectilinear Halo orbit," *The Aeronautical Journal*, Vol. 124, No. 1276, 2019, pp. 821–837. https://doi.org/10.1017/aer.2019.126.

[10] Blazquez, E., Ankersen, F., Capolupo, F., and Lizy-Destrez, S., "Convex Guidance for Close Rendezvous Operations in Cislunar Near Rectilinear Halo Orbits," *Proceedings of the 11th International ESA Conference on Guidance, Navigation & Control Systems (GNC)*, European Space Agency (ESA), Virtual Conference, 2021, pp. 1–28.

[11] Sanchez, J. C., Gavilan, F., and Vazquez, R., "Chance-constrained Model Predictive Control for Near Rectilinear Halo Orbit spacecraft rendezvous," *Aerospace Science and Technology*, Vol. 100, No. 105827, 2020. https://doi.org/10.1016/j.ast.2020.105827.

[12] Marsillach, D. A., Di Cairano, S., Kalabic, U., and Weiss, A., "Fail-Safe Spacecraft Rendezvous on Near-Rectilinear Halo Orbits," *2021 American Control Conference (ACC)*, IEEE, 2021, pp. 2980–2985. https://doi.org/10.23919/acc50511.2021.9483328.

[13] Elango, P., Vinod, A. P., Kitamura, K., Açıkmeşe, B., Cairano, S. D., and Weiss, A., "Successive Convexification for Passively-Safe Spacecraft Rendezvous on Near Rectilinear Halo Orbit," , 2025. URL https://arxiv.org/abs/2505.17251.

[14] Bucchioni, G., and Innocenti, M., "Ephemeris validation of Rendezvous Guidance in Lunar NRHO," *AIAA SCITECH 2021 Forum*, AIAA, Reston, Virginia, 2021, pp. 1–17. https://doi.org/10.2514/6.2021-0975.

[15] Woffinden, D., Shuster, S., Geller, D., and Bieniawski, S., "Robust Trajectory Optimization and GN&C Performance Analysis for NRHO Rendezvous," *Proceedings of the 2022 AAS/AIAA Astrodynamics Specialist Conference*, American Astronautical Society, Charlotte, NC, 2022, pp. 1–18. URL https://ntrs.nasa.gov/citations/20220010635.

[16] Goulet, T., Woffinden, D., Collins, N., and Andrews, B., "Robust Trajectory Design For Rendezvous in a Near Rectilinear Halo Orbit," *45th Annual AAS Guidance, Navigation and Control (GN&C) Conference*, 2023, pp. 1–25.

[17] Cavesmith, T., Woffinden, D., and Collins, N., "Angles-Only Robust Trajectory Optimization for NRHO Rendezvous," *Proceedings of the 46th Annual AAS Guidance, Navigation and Control Conference*, American Astronautical Society, Breckenridge, CO, 2024, pp. 1–23. URL https://ntrs.nasa.gov/citations/20240000556.

[18] Cunningham, D. A., Russell, R. P., and Woffinden, D. C., "Robust Trajectory Optimization for NRHO Rendezvous Using SPICE Kernel Relative Motion," *Proceedings of the 47th Annual AAS Guidance, Navigation and Control Conference*, American Astronautical Society, Breckenridge, CO, 2025, pp. 1–17. URL https://ntrs.nasa.gov/citations/20250000758.

[19] Betts, J. T., *Practical Methods for Optimal Control and Estimation Using Nonlinear Programming*, 2nd ed., Advances in Design and Control, Vol. 19, SIAM, Philadelphia, PA, 2010.

[20] Malyuta, D., Reynolds, T. P., Szmuk, M., Lew, T., Bonalli, R., Pavone, M., and Açıkmeşe, B., "Convex Optimization for Trajectory Generation: A Tutorial on Generating Dynamically Feasible Trajectories Reliably and Efficiently," *IEEE Control Systems Magazine*, Vol. 42, No. 5, 2022, pp. 40–113. https://doi.org/10.1109/MCS.2022.3187542.

[21] Breger, L., and How, J. P., "Safe trajectories for autonomous rendezvous of spacecraft," *Journal of Guidance, Control, and Dynamics*, Vol. 31, No. 5, 2008, pp. 1478–1489. https://doi.org/10.2514/1.29590.

[22] Marsillach, D. A., Di Cairano, S., and Weiss, A., "Abort-Safe Spacecraft Rendezvous in case of Partial Thrust Failure," *59th IEEE Conference on Decision and Control (CDC)*, IEEE, 2020, pp. 1490–1495. https://doi.org/10.1109/cdc42340.2020.9303782.

[23] Szmuk, M., Reynolds, T. P., and Açıkmeşe, B., "Successive Convexification for Real-Time Six-Degree-of-Freedom Powered Descent Guidance with State-Triggered Constraints," *J. Guid. Control Dyn.*, Vol. 43, No. 8, 2020, pp. 1399–1413.

[24] Uzun, S., Elango, P., Garoche, P.-L., and Açıkmeşe, B., "Optimization with Temporal and Logical Specifications via Generalized Mean-based Smooth Robustness Measures," , May 2024. https://doi.org/10.48550/arXiv.2405.10996, arXiv:2405.10996 [math].

[25] Olivares, A., Soler, M., Staffetti, E., and Bonami, P., "Multiphase Mixed-Integer Optimal Control Approach to Aircraft Trajectory Optimization," *Journal of Guidance, Control, and Dynamics*, Vol. 36, No. 5, 2013, pp. 1361–1371. https://doi.org/10.2514/1.60492.

[26] Kamath, A. G., Elango, P., Yu, Y., Mceowen, S., Chari, G. M., Carson, J. M., III, and Açıkmeşe, B., "Real-Time Sequential Conic Optimization for Multi-Phase Rocket Landing Guidance," *IFAC-PapersOnLine*, Vol. 56, No. 2, 2023, pp. 3118–3125. https://doi.org/10.1016/j.ifacol.2023.10.1444.

[27] Malyuta, D., Yu, Y., Elango, P., and Açıkmeşe, B., "Advances in trajectory optimization for space vehicle control," *Annual Reviews in Control*, Vol. 52, 2021, pp. 282–315. https://doi.org/10.1016/j.arcontrol.2021.04.013.

[28] Wang, Z., "A survey on convex optimization for guidance and control of vehicular systems," *Annual Reviews in Control*, Vol. 57, No. 100957, 2024, pp. 1–41. https://doi.org/10.1016/j.arcontrol.2024.100957.

[29] Kamath, A. G., Elango, P., Mceowen, S., Yu, Y., Carson, J. M., Mesbahi, M., and Açıkmeşe, B., "Customized Real-Time First-Order Methods for Onboard Dual Quaternion-based 6-DoF Powered-Descent Guidance," *AIAA SCITECH 2023 Forum*, 2023, p. 2003. https://doi.org/10.2514/6.2023-2003.

[30] Doll, J. A., Kamath, A. G., Smith, K. W., Harper, J. M., Rowe, I., Açıkmeşe, B., Pedrotty, S. M., and Mendeck, G. F., "Hardware in the Loop Performance of Terrestrial Powered Descent Dual Quaternion Guidance With a Custom First-Order Solver," *AIAA SCITECH 2025 Forum*, AIAA, 2025, pp. 1–27. https://doi.org/10.2514/6.2025-2776.

[31] Ross, I. M., Gong, Q., Karpenko, M., and Proulx, R. J., "Scaling and Balancing for High-Performance Computation of Optimal Controls," *Journal of Guidance, Control, and Dynamics*, Vol. 41, No. 10, 2018, pp. 2086–2097. https://doi.org/10.2514/1.g003382.

[32] Chari, G. M., Yu, Y., and Açıkmeşe, B., "Constraint Preconditioning and Parameter Selection for a First-Order Primal-Dual Method applied to Model Predictive Control," *63rd Conference on Decision and Control (CDC)*, IEEE, 2024, pp. 1676–1683. https://doi.org/10.1109/cdc56724.2024.10886050.

[33] Kamath, A. G., Elango, P., and Açıkmeşe, B., "Optimal Preconditioning for Online Quadratic Cone Programming," *IEEE Control Systems Letters*, Vol. 9, 2025, pp. 108–113. https://doi.org/10.1109/lcsys.2025.3563219.

[34] Blackmore, L., Ono, M., and Williams, B. C., "Chance-Constrained Optimal Path Planning With Obstacles," *IEEE Transactions on Robotics*, Vol. 27, No. 6, 2011, pp. 1080–1094. https://doi.org/10.1109/tro.2011.2161160.

[35] Caleb, T., Armellin, R., Boone, S., and Lizy-Destrez, S., "Chance constraints transcription and failure risk estimation for stochastic trajectory optimization," *arXiv preprint arXiv:2502.15949*, 2025.

[36] Oguri, K., and Lantoine, G., "Stochastic Sequential Convex Programming for Robust Low-thrust Trajectory Design under Uncertainty," *Proceedings of the AAS/AIAA Astrodynamics Specialist Conference*, AAS, Charlotte, NC, USA, 2022, pp. 1–20.

[37] Liu, F., Rapakoulias, G., and Tsiotras, P., "Optimal Covariance Steering for Discrete-Time Linear Stochastic Systems," *IEEE Transactions on Automatic Control*, Vol. 70, No. 4, 2025, pp. 2289–2304. https://doi.org/10.1109/tac.2024.3472788.

[38] Kumagai, N., and Oguri, K., "Robust Cislunar Low-Thrust Trajectory Optimization under Uncertainties via Sequential Covariance Steering," , 2025. https://doi.org/10.48550/arXiv.2502.01907.

[39] Echigo, K., Sheridan, O., Buckner, S., and Açıkmeşe, B., "Dispersion Sensitive Optimal Control: A Conditional Value-at-Risk-Based Tail Flattening Approach via Sequential Convex Programming," *IEEE Transactions on Control Systems Technology*, Vol. 32, No. 6, 2024, pp. 2468–2475. https://doi.org/10.1109/tcst.2024.3427910.

[40] Vinod, A. P., Weiss, A., and Di Cairano, S., "Abort-safe spacecraft rendezvous under stochastic actuation and navigation uncertainty," *60th IEEE Conference on Decision and Control (CDC)*, IEEE, 2021, pp. 6620–6625. https://doi.org/10.1109/cdc45484.2021.9683322.

[41] Dueri, D., Mao, Y., Mian, Z., Ding, J., and Açıkmeşe, B., "Trajectory optimization with inter-sample obstacle avoidance via successive convexification," *56th IEEE Conference on Decision and Control (CDC)*, IEEE, 2017, pp. 1150–1156. https://doi.org/10.1109/cdc.2017.8263811.

[42] Elango, P., Luo, D., Kamath, A. G., Uzun, S., Kim, T., and Açıkmeşe, B., "Continuous-time successive convexification for constrained trajectory optimization," *Automatica*, Vol. 180, 2025, p. 112464. https://doi.org/10.1016/j.automatica.2025.112464.

[43] Hartl, R. F., Sethi, S. P., and Vickson, R. G., "A survey of the maximum principles for optimal control problems with state constraints," *SIAM Review*, Vol. 37, No. 2, 1995, pp. 181–218. https://doi.org/10.1137/1037043.

[44] Nakamura, R., Kikuchi, J., Sasaki, T., Matsumoto, Y., Hidaka, M., Murakami, N., Ueda, S., and Satoh, N., "Rendezvous trajectory design of logistics resupply missions to the lunar gateway in near-rectilinear halo orbit," *Journal of Space Safety Engineering*, Vol. 10, No. 2, 2023, pp. 144–154. https://doi.org/10.1016/j.jsse.2023.03.001.

[45] Sagliano, M., "Performance analysis of linear and nonlinear techniques for automatic scaling of discretized control problems," *Operations Research Letters*, Vol. 42, No. 3, 2014, p. 213–216. https://doi.org/10.1016/j.orl.2014.03.003.

[46] Lew, T., Bonalli, R., and Pavone, M., "Chance-constrained sequential convex programming for robust trajectory optimization," *2020 European Control Conference (ECC)*, IEEE, 2020, pp. 1871–1878. https://doi.org/10.23919/ecc51009.2020.9143595.